JOURNAL OF GEOPHYSICAL RESEARCH, VOL. 99, NO. A4, PAGES 6351–6365, APRIL 1, 1994

Computer simulation of Alfvén waves and double layers along auroral magnetic field lines

M. Silberstein and N. F. Otani
School of Electrical Engineering, Cornell University, Ithaca, New York

Abstract. A plasma simulation has been developed to model interactions between inertial Alfvén waves and double layers and to investigate their relative contributions to auroral particle acceleration. We use a novel one-dimensional particle-in-cell code, with periodic boundary conditions, to model the nonlinear excitation of current-driven weak double layers via the free energy supplied by an inertial Alfvén wave. Analysis of the simulation output shows that double layers are not the agent primarily responsible for electron acceleration. Rather, the inertial Alfvén wave accelerates groups of electrons into a steepening beam as it encounters them. As the beam electrons reenter the main distribution, decelerated by anomalous resistive effects, they are replaced by electrons farther downstream. Hence, the particles do not free-stream over the length of the channel. Furthermore, this wave action persists even when the system is linearly stable to ion-acoustic modes, precluding the possibility that this behavior is brought about by the formation of ion-acoustic double layers.

Introduction

Since the mid-1960s, parallel electric fields have been proposed to explain the acceleration of electrons exciting the discrete aurora. Initial satellite measurements of the energy spectrum of auroral electrons above the ionospheric boundary, located at an altitude of approximately 2000 km, suggested that these precipitating particles are energized by a potential drop rather than by stochastic processes [*Swift*, 1975]. Electron velocity distributions also lead to this conclusion—so-called inverted V events have been observed on a wide range of scale lengths, from several kilometers to several hundred kilometers, and are considered an important indicator of discrete auroral activity. More recent observations by the S3-3 and Viking satellites have proven that parallel electric fields with potential drops of several keV must exist above the ionosphere, associated with upward-flowing Birkeland currents of approximately 10 $\mu A/m^2$ [*Mozer et al.*, 1980]. Current research is concerned with how these parallel electric fields are established. Both wave processes and electrostatic structures, simultaneously present in the auroral acceleration region, probably play an important role. The model used in this study incorporates mechanisms of both types in an attempt to provide insight into their relative contributions. We focus specifically on interactions between Alfvén waves and weak double layers.

Paper number 93JA02963.
0148-227/94/93JA-02963$05.00

In general, low-frequency, long-wavelength ion plasma waves, including ion-acoustic and Alfvén waves, are relevant to auroral arcs. Alfvén waves are especially relevant because they exhibit features with perpendicular scale lengths of 1-100 km, comparable to the thickness of auroral arcs. Although electron and ion cyclotron waves must be present as well, we do not address these in our model, nor are we concerned with the fine perpendicular structure of auroral arcs which has been measured as small as 100 m [*Borovsky*, 1991]. Alfvén waves are postulated as the energy source giving rise to electrostatic double layers because they originate in the magnetosphere and propagate down to the ionospheric boundary through the region where double layers are known to exist. Initial investigations of such magnetospheric-ionospheric coupling via kinetic Alfvén waves were conducted by *Goertz and Boswell* [1979], *Lysak and Dum* [1983], and *Seyler* [1988].

The role of weak double layers in auroral particle acceleration has been particularly controversial. The literature over the past decade has focused much attention on the possibility that these small-scale potential structures build up the larger parallel electric fields known to accelerate electrons along the Earth's magnetic field. So far, double-layer simulations have been unable to determine whether the double layers are actually the cause or the result of auroral electron acceleration. This is partly because the characteristics of double layers appearing in previous simulations have depended on whether an external voltage was applied and how the parallel electron drift was allowed to evolve [*Sato and Okuda*, 1981; *Barnes et al.*, 1985; *Hudson et al.*, 1987]. In general, past computational models of the evolution of microscale processes in the auroral zone have not in-

cluded the effects of these processes back on the source of the free energy driving them. Including the source of free energy is important because it affects the characteristics of the development of the microscale processes. One difficulty is that the time and length scales of the free energy (macroscale) and those of the microscale processes often do not match. Such is the case with kinetic Alfvén waves and double layers.

Our model is a useful extension of traditional electrostatic double-layer simulations in which the laws governing the evolution of the source of free energy have, up to now, been artificially and somewhat arbitrarily imposed. The solution we put forth is to specify the initial source of free energy in the form of an Alfvén wave and let the system determine the conditions and the nonlinear response naturally and self-consistently. A valuable feature of the simulation described here is the ability to simulate both phenomena simultaneously, bridging the disparity in scale lengths between the Alfvén wave and small-scale potential structures. Furthermore, the simulation treats the interaction between the double layers and the corresponding source of free energy, the Alfvén wave, in a self-consistent manner. These features will permit us to assess the relative importance of kinetic Alfvén waves and double layers in electron acceleration associated with discrete aurora.

We begin by describing the physical characteristics of the region we intend to simulate. We then present equations governing the fields, sources, and particles in this region. We briefly address the theory of obliquely propagating Alfvén waves and weak double layers in the auroral zone. We then lay out the simulation design in enough detail for the reader to appreciate the unique nature of this particular model. After this we describe the simulation parameters and output diagnostics. We then analyze the results and interpret them in the context of the physical model. Finally we summarize our findings and their implications with regard to the central issue concerning auroral electron acceleration.

Physical Model

The Current Channel

The auroral acceleration region extends from the top of the ionosphere, at 2000 km, out to 1-2 R_E. The simulated region consists of a rectangular slice of the auroral flux tube, approximately 4000 λ_D along the Earth's magnetic field (z direction), and c/ω_{pe} in the transverse (north-south, or x) direction. These figures translate to an area roughly 3 km $\times$ 80 km for $T_e/T_i = 100$. The setting of the current channel, where the double layers form, is within a much larger V-shaped potential structure, with Alfvén waves propagating on either side, as shown in Figure 1. Such potential structures are tens of kilometers wide and extend hundreds of kilometers or more along the field. We take the value of the Earth's field at 1 R_E to be 0.063 G and estimate the density at $1R_E$ (along high-latitude field lines lying outside the plasmasphere) to be $n = 10\text{cm}^{-3}$. Another important parameter is the ratio of plasma pressure to magnetic field pressure, known as the plasma beta, $\beta = p_e/(B^2/8\pi)$, which, for these parameters, is much less than m_e/m_i. Our model extends that of *Goertz and Boswell* [1979] for a similar low-beta plasma at an altitude of 4000 km.

Physical Equation Set

The model we present here is a microscopic description of the auroral zone plasma, omitting cyclotron motion. Maxwell's equations with background magnetic field $\vec{B}_o = \hat{z}B_o$ and wave fields $\vec{E} = \hat{x}E_x + \hat{z}E_z$ and $\vec{B} = \hat{y}B_y$ are

$$\partial_x E_x + \partial_z E_z = 4\pi\rho \tag{1}$$

$$\partial_z E_x - \partial_x E_z = -\frac{1}{c}\partial_t B_y \tag{2}$$

$$\partial_x B_y = \frac{1}{c}\partial_t E_z + \frac{4\pi}{c}J_z \tag{3}$$

$$\partial_z B_y = -\frac{4\pi}{c}J_x \tag{4}$$

where we have neglected the transverse component of the displacement current.

The sources are defined below. The full nonlinear kinetic particle motions within the current channel make up J_z:

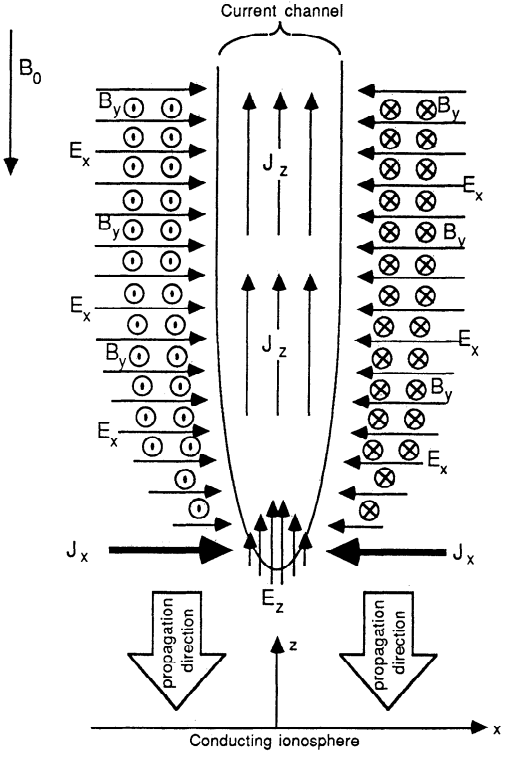

Figure 1. Location of the simulation region with respect to a V-shaped potential structure. The field-aligned electron current within the channel is fed by transverse ion polarization currents, induced by the time-varying electric field superimposed on the Earth's background magnetic field. A return current outside the channel is assumed to close the current loop.

$$J_z(z,t) = n_o \sum_{s,i} q_s v_{si}(t) \delta(z - z_i), \quad (5)$$

where s refers to the species, i is the particle index, and δ is the Dirac delta function. The particle velocities are governed by the force equation,

$$\frac{dv_{si}(t)}{dt} = \frac{q_s}{m_s} E_z, \quad (6)$$

where $dz_{si}/dt = v_{si}$. The continuity equation, with $\vec{J} = \hat{x}J_x + \hat{z}J_z$,

$$\partial_t \rho = -\partial_x J_x - \partial_z J_z \quad (7)$$

suggests associating a "parallel charge density" with J_z and a "perpendicular charge density" with J_x. Physically, since the charge flowing into the channel from either side is produced by polarization drift, we define

$$\rho_\perp \equiv -\frac{c^2}{4\pi v_A^2} \partial_x E_x \quad (8)$$

Then $\rho_\parallel \equiv \rho - \rho_\perp$. It will prove useful to make this separation, because $\rho_\parallel$ and $\rho_\perp$ are represented differently in the simulation. We have now defined all the physical quantities we are modeling and the equations governing them. The system is linear with the exception of (5), which allows for observed nonlinear kinetic effects such as double layers.

Obliquely Propagating Alfvén Waves

There are several varieties of Alfvén waves which have a strong propagation component perpendicular to the background field. In a low-beta plasma, it is appropriate to consider the effect of finite parallel electron inertia, which gives rise to one type of obliquely-propagating Alfvén wave.

Linearizing (1) – (8) in the low-beta limit ($\beta \ll m_e/m_i$), we obtain a biquadratic dispersion equation

$$\omega^2(\omega^2 - \omega_{pe}^2) + k_z^2 v_A^2(\omega_{pe}^2 - \omega^2) - \omega^2 k_x^2 c^2 = 0 \quad (9)$$

Solving for ω^2, we find that an inertial Alfvén wave having dispersion relation

$$\omega^2 = \frac{k_z^2 v_A^2}{1 + (k_x c/\omega_{pe})^2} \quad (10)$$

comes from the negative branch of the quadratic formula, using the approximations $\omega_{pe}^2 \gg k_z^2 v_A^2$ and $k_x^2 c^2 \gg k_z^2 v_A^2$. As there is nothing kinetic about this wave, we prefer to call it the "inertial Alfvén wave" while reserving the term "kinetic Alfvén waves" for other waves, obtained in the high-beta limit, consistent with *Seyler* [1988]. Since the electrons in the acceleration region fall within the inertial regime ($\beta < m_e/m_i$), we will not discuss further the kinetic Alfvén waves, but refer the reader to the papers of *Stefant* [1969], *Hasegawa* [1976], *Hasegawa and Chen* [1975], and *Hasegawa and Sato* [1982] We also find that ordinary ("O mode") electromagnetic waves,

$$\omega^2 = \omega_{pe}^2 + k_x^2 c^2 \quad (11)$$

emerge from the positive branch of Eq. (9).

Double Layers

Prominent among the nonlinear effects we observe are double layers. Typical separation distances between double layers seen in simulations are 100-1000 Debye lengths. There is little doubt that double layers exist—they have been observed consistently in both ionospheric and laboratory plasmas [*Chan et al.*, 1984]. The most often cited observations of double layers are those seen in 1976 in the auroral zone by the American S3-3 satellite [*Temerin et al.*, 1982] and the 1986 Swedish Viking satellite [*Bostrom et al.*, 1988]. A typical double layer has scale length $\approx 10\lambda_D$ and maintains its shape on timescales of order ω_{pi}^{-1}. We believe that the double layers observed in the auroral acceleration region are current driven, and we categorize them as weak double layers, supporting potential drops less than T_e/e.

Standard double-layer theory describes how the plasma particles behave when they encounter these structures. Once a potential discontinuity is introduced in the plasma, four particle populations are required to sustain the typical double-layer structure shown in Figure 2. Electrons entering from the right are reflected by a potential hill and form a region of trapped particles, as do ions coming from the left. Electrons entering from the left are accelerated through the potential drop, as are ions approaching from the right. This action results in a net energy gain for both species of particles. Double-layer formation must occur in any simulation of the auroral zone which treats accurately the microscopic particle dynamics.

Simulation Model

The simulation is a one-dimensional particle-in-cell code, which may be regarded either as an Alfvén wave propagation model including full kinetic parallel particle dynamics or as an essentially electrostatic double layer simulation (e.g., ES1 [*Birdsall and Langdon*, 1985]) in which external conditions are self-consistently determined through a simple inertial Alfvén wave model.

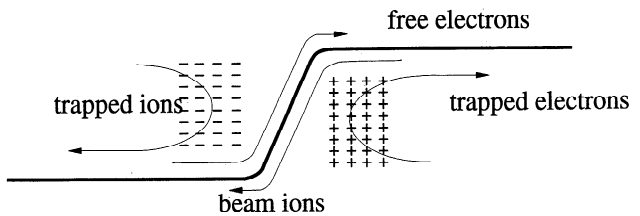

Figure 2. Monotonic double-layer potential structure. Electrons entering from the right are reflected by a potential hill and form a region of trapped particles, as do ions coming from the left. Electrons moving from the left are accelerated through the potential drop, as are ions approaching from the right.

The boundary conditions in the x-direction are periodic and are specified by the fixed input parameter k_x, where $k_x = 0$ corresponds to an infinitely wide channel or $k_x c/\omega_{pe}$ in (10) is of order 1 for the case of inertial Alfvén waves. For a channel of finite perpendicular extent, k_x is nonzero, requiring the presence of the parallel electric field E_z, which is then available to accelerate electrons [*Otani*, 1991]. The particle boundary conditions in the z-direction are also periodic, in the sense that particles which leave the system at one end reenter at the other. All field quantities are periodic at the boundaries, except for the potential, which may sustain a net difference across the system. Alfvén waves and double layers were simulated by *Goertz et al.* [1991] in two dimensions for an artificially short system (150 Debye lengths) with nonperiodic boundary conditions in z, whereas our one-dimensional periodic simulation extends 4096 Debye lengths in the z direction.

The simulation effectively has two principal parts. One part models the propagation of the inertial Alfvén wave. The wave is assumed to consist of a specific sinusoidal standing wave in the x direction but allows traveling waves with arbitrary dependence on z and t in the z direction. A crossing pair of obliquely propagating Alfvén waves superpose to form a single wave effectively propagating along the field. The forms of the currents and fields are chosen so as to maximize the parallel current and electric field within the channel at $x = 0$, while the transverse fields associated with the Alfvén wave are maximized outside the channel, where the wave propagates. Thus, we assume

$$E_x = \hat{E}_x(z,t)\sin k_x x \quad (12)$$

$$B_y = \hat{B}_y(z,t)\sin k_x x \quad (13)$$

$$J_z = \hat{J}_z(z,t)\cos k_x x \quad (14)$$

$$E_z = \hat{E}_z(z,t)\cos k_x x \quad (15)$$

where k_x is the specified constant. Likewise, the charge densities and the potential associated with the parallel electric field exist within the channel and so have the form

$$\rho_{\|} = \hat{\rho}_{\|}(z,t)\cos k_x x \quad (16)$$

$$\rho_{\perp} = \hat{\rho}_{\perp}(z,t)\cos k_x x \quad (17)$$

and

$$\phi = \hat{\phi}(z,t)\cos k_x x. \quad (18)$$

The equations relating the wave quantities are Ampère's law and Faraday's law. For $k_z = 0$, these are written as

$$\langle\hat{E}_z\rangle_{n+1} = \langle\hat{E}_z\rangle_n - 4\pi\Delta t\langle\hat{J}_z\rangle_{n+1/2} + c\Delta t k_x\langle\hat{B}_y\rangle_{n+1/2} \quad (19)$$

$$\langle\hat{B}_y\rangle_{n+1/2} = \langle\hat{B}_y\rangle_{n-1/2} - \left(\frac{k_x c}{\omega_{pe}}\right)^2 \frac{v_A}{v_{the}}\langle\hat{E}_z\rangle_n \Delta t \quad (20)$$

where

$$\langle\hat{J}_z\rangle = \frac{n_o}{N_p}\sum_s q_s \sum_i v_{zis} \quad (21)$$

is calculated from the particle portion of the code (see below), $\langle\rangle$ denotes the spatial average in z, and the subscript n is the timestep index. For $k_z \neq 0$, the counterpart to (20) is

$$\hat{B}_{y,n+1/2}(k_z) = \hat{B}_{y,n-1/2}(k_z) + \omega_{pe}\Delta t k_z v_A \hat{\rho}_{\perp,n}(k_z) - \left(\frac{k_x c}{\omega_{pe}}\right)^2 \frac{v_A}{v_{the}}\hat{E}_{z,n}(k_z)\Delta t \quad (22)$$

The additional term contains the perpendicular charge density, given by

$$\hat{\rho}_{\perp,n+1}(k_z) = \hat{\rho}(k_z)_{\perp,n} + k_z v_A \hat{B}_{y,n+1/2}(k_z)\Delta t \quad (23)$$

Information about the particle motion is contained in the current and electric field terms. Note that $\rho_{\perp}$ may be thought of as essentially E_x, in view of (8).

The second part of the simulation addresses the parallel plasma response to the wave. The numerical set of equations governing this part of the code is as follows:

$$\hat{\rho}_{\|}(z) = n_o \frac{N_g}{N_p}\sum_s q_s \sum_i S(z - z_{is}) \quad (24)$$

$$\hat{\phi}(k_z) = \frac{4\pi}{k_z^2}[\hat{\rho}_{\|}(k_z) + \hat{\rho}_{\perp}(k_z)] \quad (25)$$

$$\hat{E}_z(k_z) = -ik_z\hat{\phi}(k_z) \quad (26)$$

$$v_{z,n+1/2} = v_{z,n-1/2} + \frac{q\hat{E}_{z,n}(z_{is})}{m}\Delta t \quad (27)$$

$$z_{n+1} = z_n + v_{z,n+1/2}\Delta t \quad (28)$$

where N_g is the number of grids, N_p is the number of particles, and S is the first order shape function, weighting particles to the grid [*Birdsall and Langdon*, 1985]. In each equation, the $\sin k_x x$ or $\cos k_x x$ terms cancel, leaving just the amplitudes, denoted by the "hat," e.g., $\hat{E}$. We determine $\hat{E}_x$ indirectly by first solving for $\hat{\rho}_{\perp}$ and then using

$$\hat{E}_x = \hat{\rho}_{\perp}\frac{4\pi v_A^2}{k_x c^2} \quad (29)$$

We note that $\rho_{\|}$ is a particle quantity, whereas $\rho_{\perp}$ is a grid quantity. This part of the simulation resembles a standard electrostatic electron-and-ion particle simulation (e.g., the well-known ES1 code [*Birdsall and Langdon*, 1985]), but it couples to the inertial Alfvén wave physics through the presence of a z-averaged parallel electric field $\langle E_z\rangle$ and the ion polarization drift charge density, $\rho_{\perp}$. We emphasize that the simulation maintains the presence of the Alfvén wave in the channel self-consistently. We do not inject currents or impose a potential across the system — the fields are determined exclusively by the particle motion, which is in turn influenced by the Alfvén wave.

Linear stability analysis of the simulation equations yields, ignoring aliasing, the following dispersion relation

$$(\omega\alpha)^4 - (\omega\alpha)^2[\omega_{pe}^2 N_g^2 S_{kz}^2 + k_z^2 v_A^2 + k_x^2 c^2] = -\omega_{pe}^2 v_A^2 k_z^2 N_g^2 S_{kz}^2 \quad (30)$$

where $\alpha = \sin(x)/x$ with $x = \omega\Delta t/2$, for $\omega\Delta t \ll 1$ and $k_z\Delta z \ll 1$. We can guarantee linear stability of the simulation when $(\Delta t)^2 \leq 4/(k_x^2c^2 + k_z^2v_A^2 + \omega_{pe}^2N_g^2S_{kz}^2)$. This implies that linear stability is ensured if the following three conditions are met: $\Delta t \leq 2/(\omega_{pe}N_gS_k\sqrt{3})$, $\Delta t \leq 2/(k_xc\sqrt{3})$, and $\Delta t \leq 2/(k_zv_A\sqrt{3})$. Here, S_{kz} is the spatial Fourier transform of the particle shape factor $S(z)$. This criterion is specific to the set of physical equations used in the simulation, and assumes that the simulation employs a grid.

Results

Early runs of the code [*Otani*, 1991] revealed the formation of double layers in the channel when the electrons initially are given a drift velocity with respect to ions. This initial condition effectively replaces the inertial Alfvén wave, giving rise directly to the ion-acoustic instability. This is equivalent to the situation that would exist after the wave has traveled through the channel, reflected off the conducting ionosphere, and passed back through the channel again. Meanwhile, the physics of the regions flanking the channel are held consistent with the presence of an inertial Alfvén wave. Results from these first trials, with an infinite channel width, showed that the parallel current in the channel was maintained self-consistently at a constant value by the generation of a parallel electric field produced as a consequence of the Alfvén wave physics. A second trial, performed with a finite channel width, showed a decay in the parallel current as a result of anomalous resistivity supplied by the double layers.

The next logical step was to produce current-driven double layers by applying a perturbation in the form of a downward-propagating inertial Alfvén wave, rather than by simply forcing the electron drift. If the parallel electron drift associated with the inertial Alfvén wave exceeds the electron thermal velocity, we would again expect an ion-acoustic instability, leading to the formation of double layers. The drift velocity clearly depends on the wave amplitude. Unfortunately, when the amplitude is large enough to generate double layers, it already exceeds the value at which strongly nonlinear Alfvén wave behavior sets in, thereby disrupting observation of the ensuing microscale effects. One of our primary tasks, therefore, was to initiate a well-behaved, 'clean', though still technically nonlinear, inertial Alfvén wave so that subsequent interaction with double-layer phenomena could readily be studied.

Initializing such a wave necessitated a careful treatment of the initial particle positions. Initializing the particle perturbations according to linear theory does not allow the cancellation of higher-order terms in the charge density. The quasi-neutrality condition required for the propagation of the Alfvén wave is thus not satisfied. More specifically, recall that $\rho_\parallel$ is the charge density resulting from particle motion along the background magnetic field and $\rho_\perp$ is the ion polarization charge density arising from ion flow across the field. The value of $\rho_\perp$ is calculated to first order in the wave amplitude, whereas the value of $\rho_\parallel$ is determined by the particle positions, obeys the continuity equation, and includes higher-order terms. When calculating the Fourier components of the potential according to (25), most of the the first-order mode cancels, because the two components of charge have nearly equal and oppositely directed first-order terms. However, initially there is no $\rho_\perp$ contribution to the second-order mode, and therefore mode 2 cancellation does not occur. Thus, the charge density is dominated by the large second-order contribution of $\rho_\parallel$, and the resulting potential is inconsistent with the mode 1 Alfvén wave we seek to initialize before any time-stepping has even begun.

An improved initialization scheme is achieved by first assuming the desired form of the number density, n, inserting it into the exact expression describing the modification of the density under a spatially dependent displacement profile, and then solving for the displacement that will yield the desired density perturbation. Since this scheme is one of the unique aspects of the simulation model, we describe it here in more detail.

Suppose, before a displacement $\xi(z)$ is applied, there is a density $n_o(z_o)$ in the region between z_o and $z_o + dz$. After the displacement, the particle at z_o has moved to $z_o + \xi(z_o)$ and the particle at $z_o + dz$ has moved to $(z_o + dz) + \xi(z_o + dz)$ (Figure 3). Define this new density to be n_1. The equation

$$n_o(z)dz = \tag{31}$$
$$n_1(z + \xi(z))[z_o + dz + \xi(z_o + dz) - (z_o + \xi(z_o))]$$

is a statement of the conservation of particles through such a displacement. Simplifying (), we arrive at an exact expression for n_1,

$$n_1(z + \xi(z)) = \frac{n_o(z)}{1 + d\xi(z)/dz} \tag{32}$$

We require that this density profile contain our mode 1 perturbation. Assume then that n_o is constant and

$$n_1(z + \xi) = n_o + \delta \cos k_z(z + \xi), \tag{33}$$

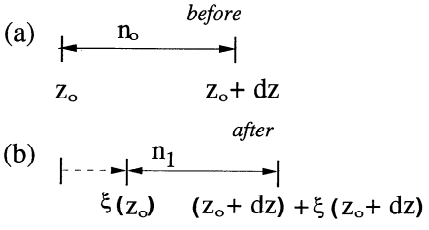

Figure 3. Diagram of a one-dimensional spatial particle distribution, as it is displaced by an applied force. Different particles are displaced by different amounts, but the number of particles remains constant from (a) to (b).

From Eq. (33) we can solve for the displacement required to produce this n_1,

$$\xi = \frac{-\delta}{n_o k_z} \sin k_z(z+\xi) \tag{34}$$

Then (34) is solved iteratively for ξ, until the result is accurate to within roundoff.

These initial particle displacements, along with parameters obeying the stability criterion, produced both the desired inertial Alfvén wave and double layers coexisting simultaneously in the simulated auroral current channel. Of the many runs we tried, the representative examples presented here had the the following simulation input parameters: $v_A/v_{the} = 3.33$, $v_d/v_{the} = 1.0$, $\omega_{pe}\Delta t = 0.12$, $\lambda_D/\Delta z = 1.0$, $k_x c/\omega_{pe} = 1.0$, $T_e/Ti = 100$, $m_i/m_e = 100$, $\beta_e = 2(m_e/m_i)(v_{the}/v_A)^2 = 0.0018$. The parallel length of the channel is interpreted either as several thousand Debye lengths long or one inertial Alfvén wavelength long. We should mention that, having created drift motion in the system by launching the inertial Alfvén wave, we superimposed the original constant drift, since observations suggest that both sources of particle drift motion exist. We ran the simulation with these parameters several times, using various diagnostics to extract physically meaningful results.

The simulation results were displayed in the form of a computer movie. Movie frames depict the following quantities. The scatter plots are phase space (v_z versus z) graphs of electrons and ions, respectively; below these we plot the field quantities associated with the Alfvén wave, showing amplitude versus position in the z direction. Motion in the positive z direction corresponds to downward motion along the field. We can monitor the wave via either the potential or the magnetic field component B_y. In Figure 4 the electrons initially are drifting at the thermal speed with respect to the cold ions, and we note that one Alfvén wavelength is contained in the system. After only 160 ω_{pe}^{-1} we already observe bunching in the particle distributions. Sharp structures, a signature of double layers, are forming at the left, where the peak amplitude of the wave is positioned (Figure 5).

Figure 6 shows the potential structures of the double layers and their associated phase space ion holes. It also indicates that the particles have undergone significant heating. A significant decrease in the amplitude of the potential away from the double layers indicates that energy has been lost from the wave and has presumably gone into heating the particles.

These double layers are correlated with the structures shown in Figure 7, a series of greyscale plots of the potential history throughout the system. As in the scatter plots, the most interesting features occurred at the ends of the system for this initial run. At the far left, the dark herringbone pattern corresponds to what we call an 'ion-acoustic explosion'. Emanating from this area are ion-acoustic waves and double layers appearing as diagonal lines and light, curved features, respectively. Darker areas signify regions of positive potential preceded by a negative potential dip, manifested by white shadows on the left border. The curves trace the dip/rise (cf. Figure 6) double-layer structures as they travel characteristically to the right, stop, and move

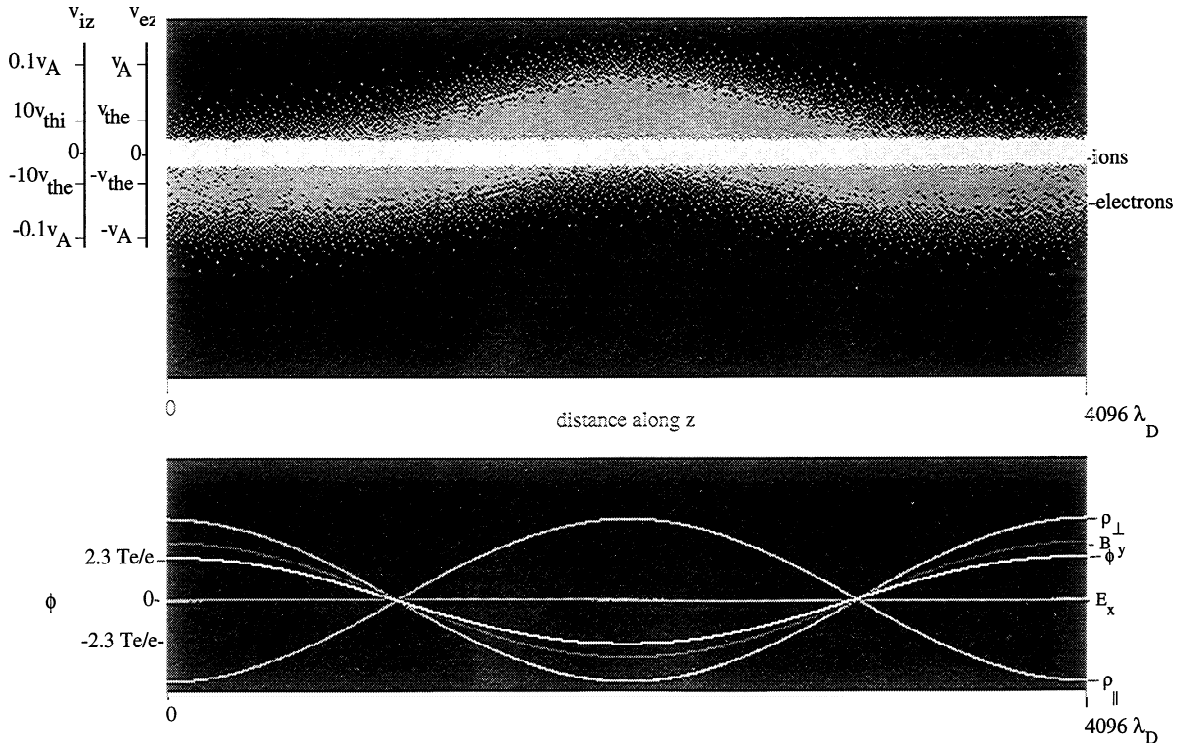

Figure 4. Initial conditions, for $T_e = 100T_i$. Electrons are initialized with a Maxwellian velocity distribution and a superimposed sinusoidal drift.

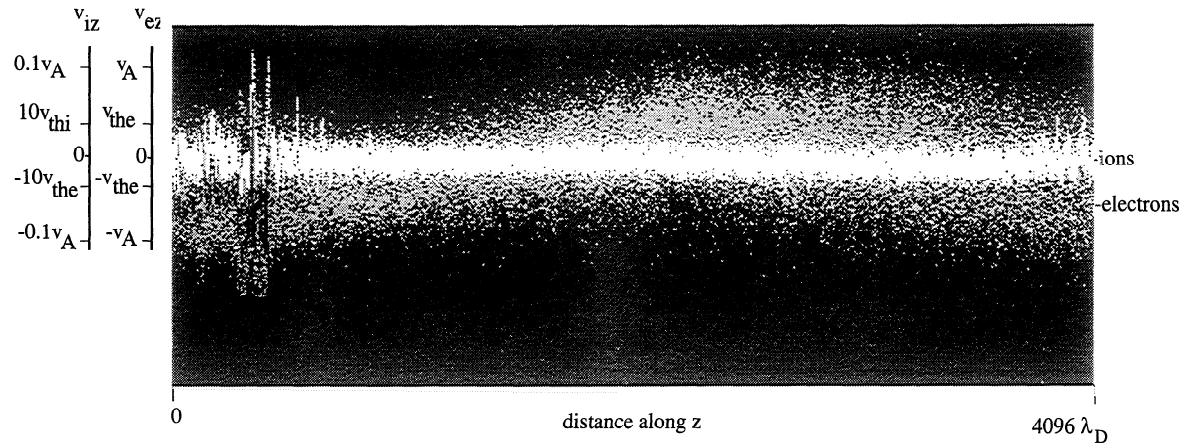

Figure 5. Double layers appearing at left, at 0.13 of the total simulation time,which is 1200 ω_{pe}^{-1}.

back to the left. At the other end of the system the double layers travel in the opposite direction and then also stop and change direction. The duration of a typical double layer in our runs is 190 electron plasma periods ($\tau_e = (1/10)\tau_i$). We observe up to 10 double layers within 4096 λ_D, whereas others typically have observed only 4 in the same length system [*Sato and Okuda*, 1981]. Looking closely at the middle of the system, the light and dark diagonal bands represent the Alfvén wave, propagating at constant velocity. We can also see evidence of ordinary electromagnetic waves, experienced by the particles as enhanced plasma oscillations. These waves are strongly nonlinear and are manifested along the top of the greyscale plot as black and white horizontal stripes. They eventually disappear, presumably as a result of Landau damping. Even though we have averaged over the plasma oscillation timescale (i.e., each stripe represents multiple cycles) in the greyscale plot (Figure 7), the oscillations are still large enough to show up early in the simulation.

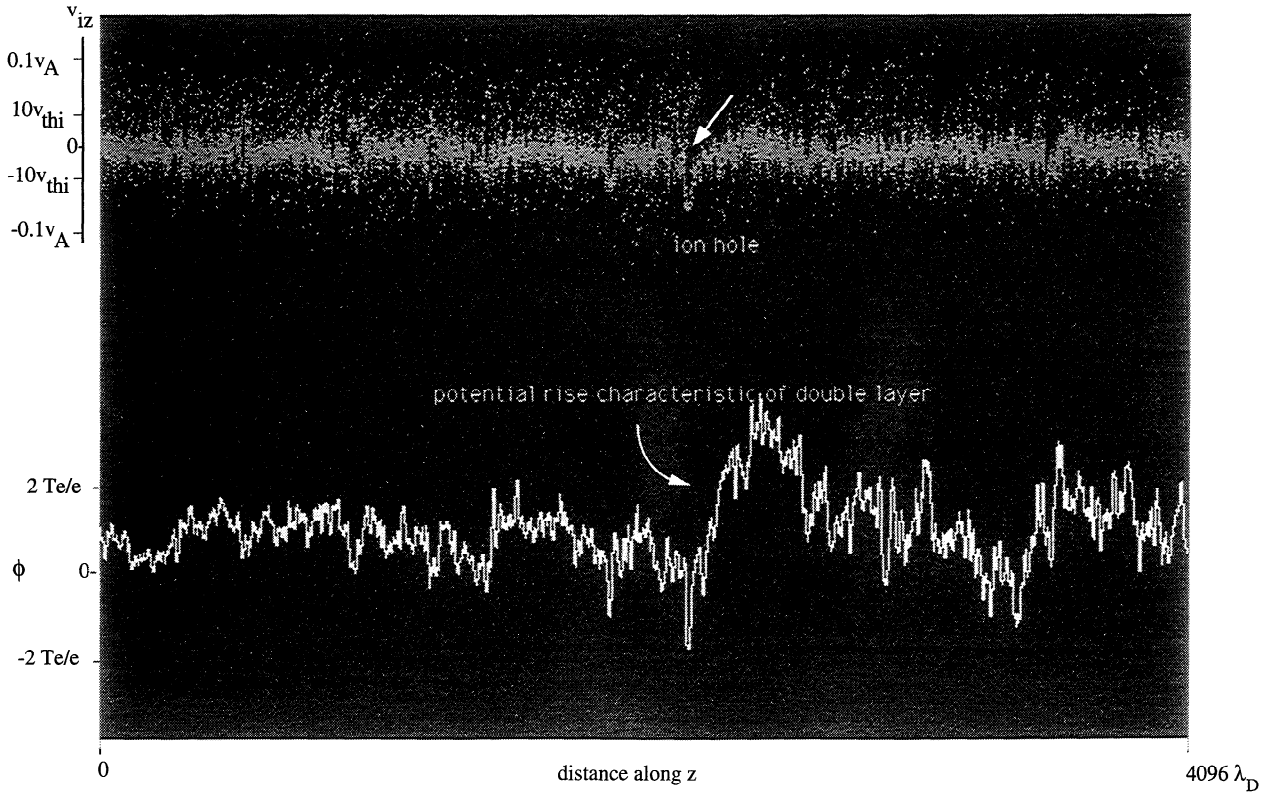

Figure 6. Double-layer potential is characterized by a dip followed by a sharp rise. This corresponds to a depletion in the ion population.

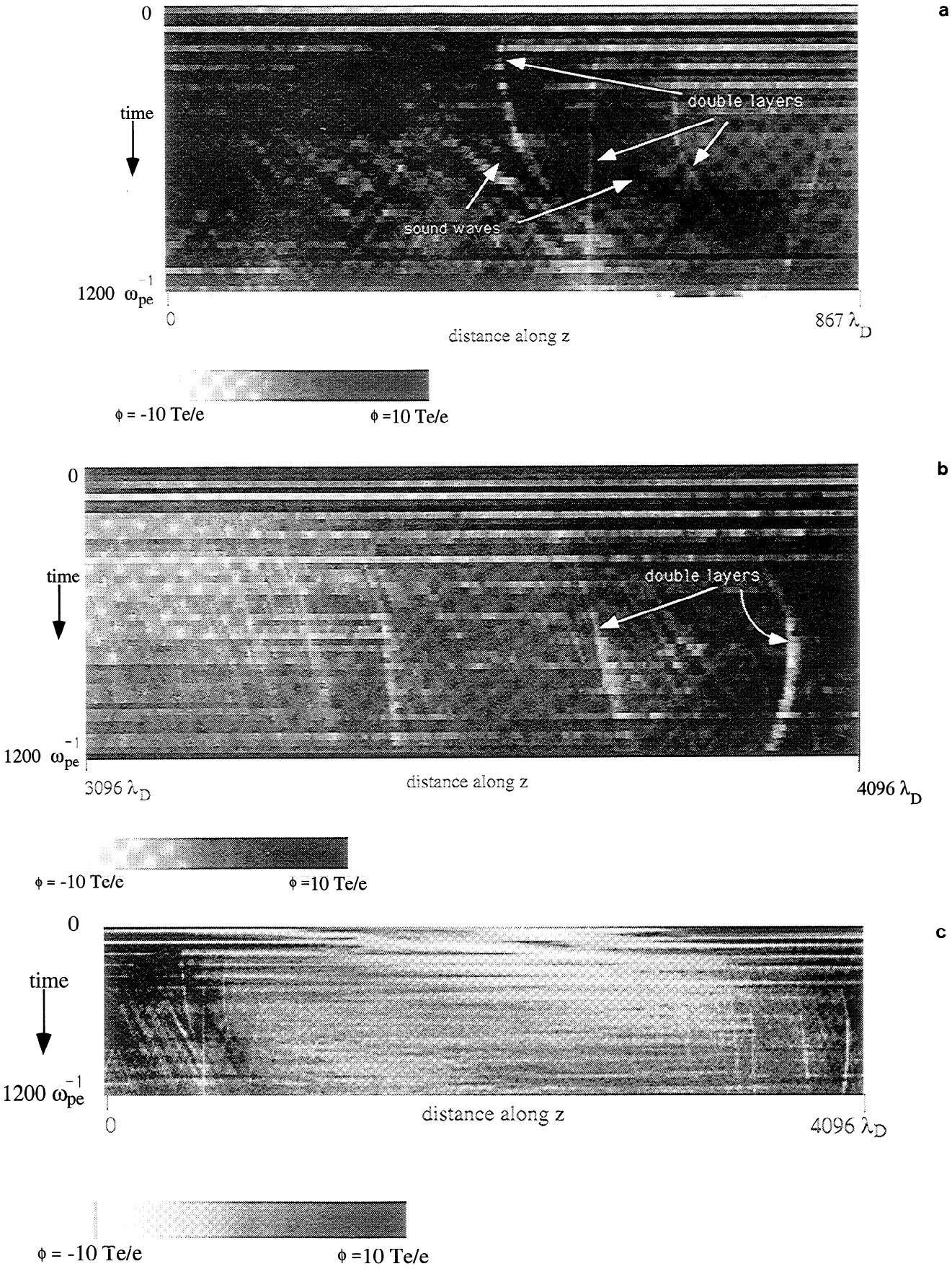

Figure 7. Potential history plots showing double- layer structures. The intensity of the potential is represented as a greyscale value (black is high potential) on a time versus space graph. (a and b) Magnifications of the ends of the system; (c) Whole system.

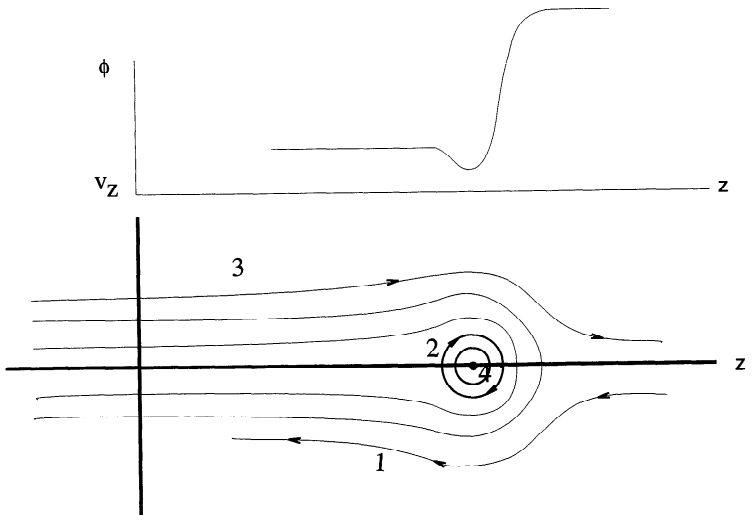

Figure 8. Ion-acoustic double-layer potential structure. (1) Ions accelerating to the left; (2) ions trapped in the potential dip, (3) high-energy ions decelerated by the hill; (4) stationary ions trapped in the dip.

Interpretation

These simulations raised many questions about the details of the wave behavior, the generated potential structures, and their mutual interactions. We attempt to answer some of these questions in this section and to relate our discoveries to the auroral zone.

Particle Trajectories

As we have shown, the small-scale structures observed in the channel coincided with sharp potential drops, ion hole formation, and features in the greyscale potential history. These are typically recognized as evidence of double layers. However, a more detailed analysis of the phase space picture is desirable for complete confidence that these structures were double layers. Unequivocal proof of the presence of double layers is found by identifying the signature particle populations required to sustain them. Figure 8 is a schematic of a modified idealized double layer, with a potential dip, characteristic of weak double layers, occurring immediately before the sharp rise. Also shown are the ion phase space trajectories one would expect to observe.

We would expect to see three of the four possible ion trajectories. There are no deeply trapped ions (population 4) in this simulation, because the particles do not experience collisions sufficient to fully deplete their potential energy. Thus, this region of phase space is empty, forming an ion hole.

Density depletions characteristic of ion holes have been observed by the Viking satellite and have been studied in depth by *Tetrault* [1988]. A typical depletion observed by Viking measured 10-50 λ_D along the field and had a velocity on the order of the sound speed, $c_s = (T_e/m_i)^{1/2}$. Figure 9 depicts an ion hole produced by the simulation code. The white dots are the trajectory of a population 2 ion, surrounding an ion hole of diameter 45 λ_D. Since the ion hole is a region of negative potential, it causes a depletion of electrons as well. Leftward accelerating ions, forming U-shapes

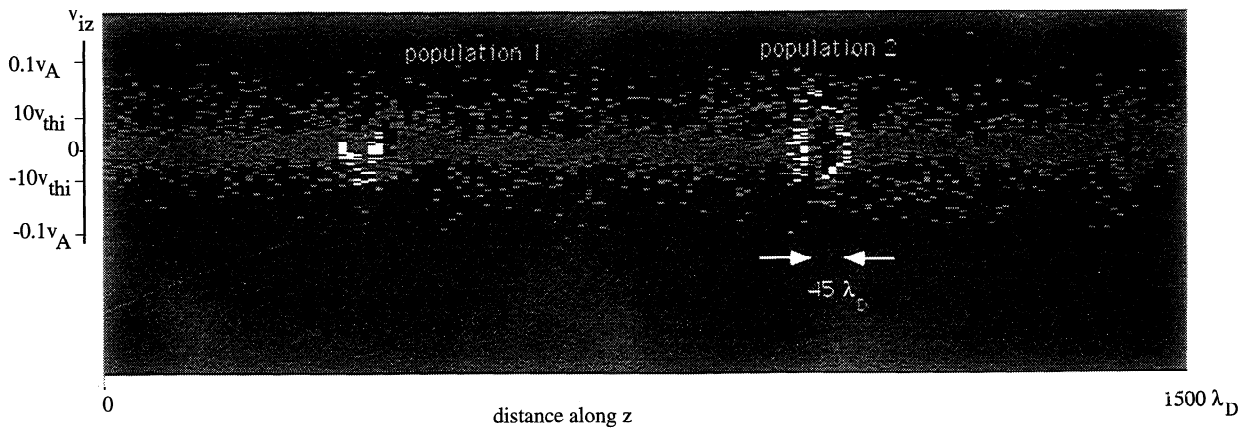

Figure 9. Magnification of ion holes (right) with trajectories of ion populations 1 and 2.

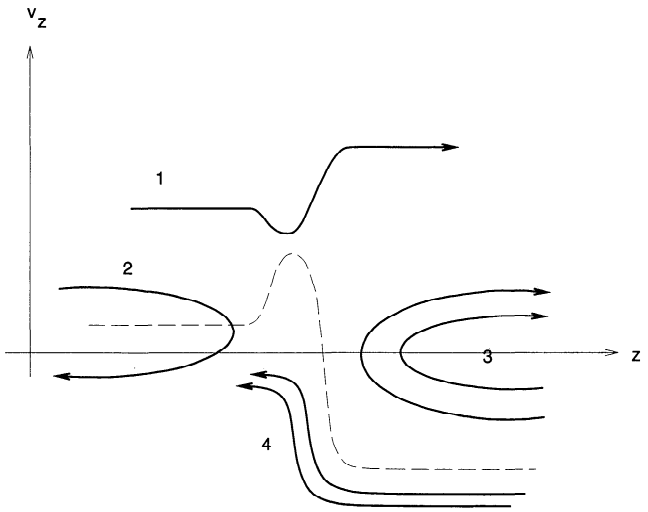

Figure 10. (1) Electrons are decelerated by the potential dip and then accelerated by the hill; (2) electrons from the left reflected by the dip; (3) electrons from the right turned around by the hill; (4) electrons from the right are decelerated. The dotted line shows the potential as seen by the electrons—the reverse of the ion potential structure.

around the ion hole, indicative of population 1, are also shown in Figure 9. Rightward drifting ions (population 3) were also observed.

Expected electron phase space trajectories are indicated in Figure 10. Again, there are four populations, but none of them are trapped. The electron trajectories were much more dynamic than those of the ions, because of the large mass difference. The electrons traversed a much greater portion of the system and their trajectories quickly overlapped. Figure 11 shows some early electron trajectories. The electrons are observed to fall into regions where they circulate for a few plasma periods before being forcefully ejected. When this occurs, they drift quickly to the right until they become trapped again. Although the asymmetric double-layer model (Figures 8 and 10) does not allow for electron trapping per se, the electrons can be constrained between two successive potential structures, acting as population 3 on one side and population 2 on the other.

Both sets of particle trajectories reveal clearly that the double layers are instrumental in energizing ions but not in accelerating electrons overall, at least not on scales larger than the width of a double layer. This is consistent with satellite data since, although double layers have always been correlated with upward flowing ions [*Mälkii et al.*, 1992], experimental evidence for a connection between double layers and downward-streaming electrons is less clear. Furthermore, we observed ions, located away from double layers, simply bobbing up and down as the Alfvén wave intercepts them, responding only when they encounter a double layer. The electrons are observed to move about two orders of magnitude faster across the system, displaying intermittent acceleration/deceleration behavior. This motion is associated with the inertial Alfvén wave action and turbulence, not with double layers.

Interaction of the Alfvén Wave with Electron Distribution

We then analyzed the electron phase space distribution. Initially sinusoidal, it soon was observed to form a beam with a steep-edged front. This front is consistently preceded by a rise in the local potential, as shown in Figure 12. Double layers are left in the wake of the front. At first, it seemed that the steepening of the beam front might be explained by the natural tendency of the faster electrons to travel farther than the slower ones in the same period of time, as illustrated in Figure 13. However, the steepening occurs only in the upper half-plane of phase space, where the velocities are positive and the electrons are moving to the right. The distribution of left-moving (backwards flowing) electrons does not show a similar steepening, which led us to suspect that it was not simply a ballistic effect.

We also observed selective electron acceleration; i.e., not all the electrons end up in the beam. The electron velocity distribution changed, but the mean particle displacement was relatively small. While the Alfvén wave travels across the system, a distance equal to one Alfvén wavelength, Figures 14 and 15 show that individual electrons travel only about one-quarter of the system length. Those starting out at the left end of the system were still in the same general area at the end

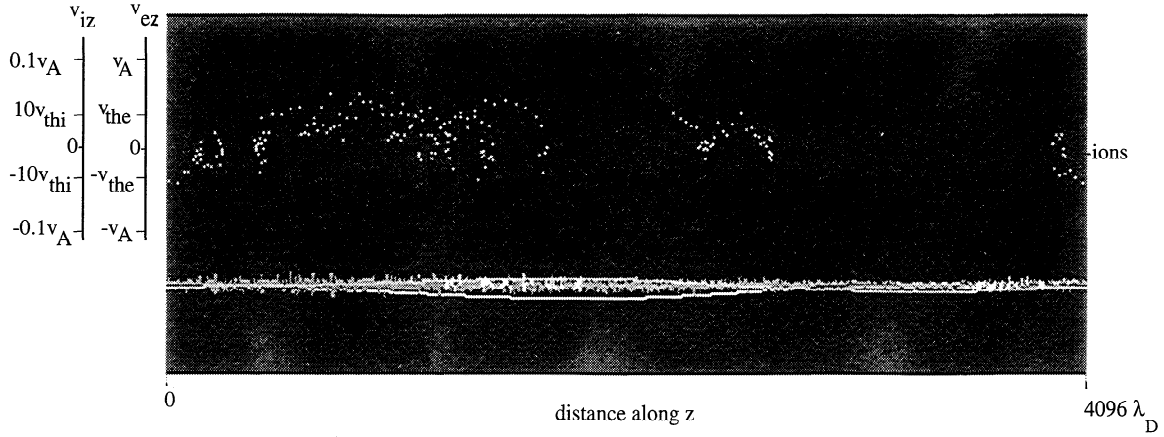

Figure 11. Right-moving electron trajectories.

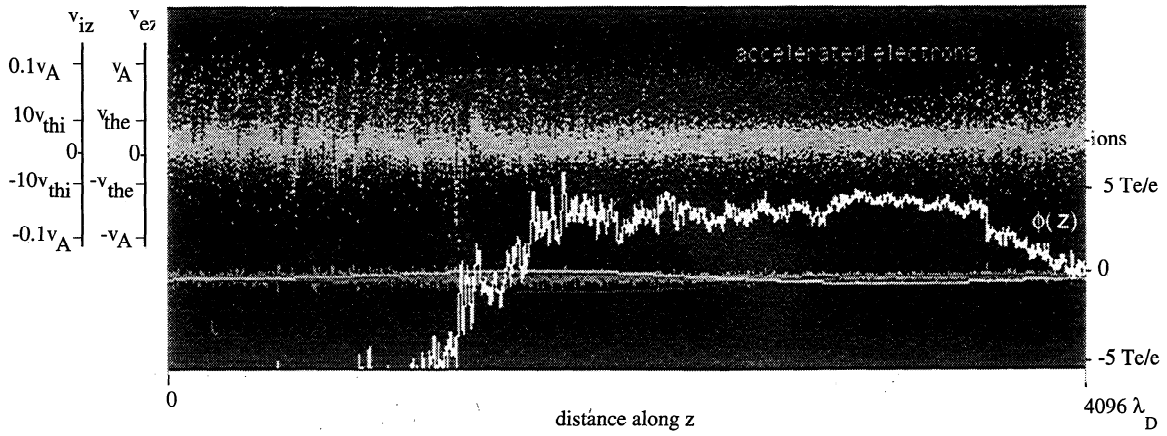

Figure 12. Overall system showing electron beam traveling along the channel length.

of the simulation, as were the ones in the middle and on the right. The slowest electrons experienced significant heating and were accelerated into the beam, while the fastest electrons were initially decelerated. The initial delineations in speed are lost as successive groups of electrons are locally accelerated into the beam by the Alfvén wave and then decelerated by turbulent processes, causing them to return to the main distribution. While the average velocity taken over a small region coinciding with the Alfvén wave front shows electron acceleration, the average electron velocity over the whole system, and therefore the current, $J = nev$, decreases in time, as it must to remain consistent with the previously observed current decay discussed by *Otani* [1991] for the case when $k_x \neq 0$. This is attributed to magnetic diffusion made possible by the resistive effects of the double layers.

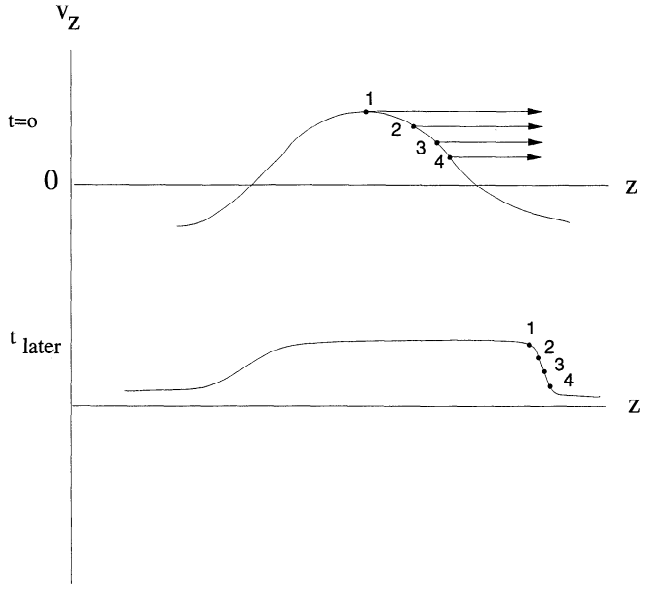

Figure 13. Hypothesized "ballistic" electron motion. Given their initial velocities, with no force from the wave, we would see a steep-edged front form as the fast particles catch up with the slower-moving particles placed ahead of them. This situation was not observed.

We conclude that particles, though apparently swept quickly across the system, are, in fact, not traveling ballistically. We suspect that when this mechanism is active, electrons thought to descend from altitudes as high as the plasma sheet into the neutral atmosphere actually originate at a much lower altitude, where they are picked up and accelerated by the Alfvén wave. Electrons forming the precipitating population must originate near the bottom of the acceleration region, because those particles energized at higher altitudes would have already been recycled back into the main distribution. The electrons thus behave in a manner similar to electrons carrying current in a wire, where charges need not move far from their origin.

The Ion-Acoustic Instability

The ion-acoustic instability as a generator of current-driven double layers has been studied by *Hudson et al.* [1983], *Sato and Okuda* [1981], and *Hasegawa and Sato* [1982]. Ion-acoustic waves with $c_s = \sqrt{T_e/m_i}$ occur in plasmas where the electron temperature exceeds the ion temperature and may become unstable if there exists a large enough electron drift with respect to ions. In our case, the necessary drift is produced by the downward propagating inertial Alfvén wave. The ion-acoustic instability in turn supplies free energy to drive weak double layers in the current channel.

Recent rocket flights indicate that, in the auroral zone, it is more likely that $T_e \approx T_i$, a condition inhibiting the development of the ion-acoustic mode. *Koskinen et al.* [1990] note that it is crucial to determine, but difficult to measure, T_e and T_i in the weak acceleration regions where solitary structures such as double layers have been observed. However, their data show that the ion temperature at 8000-11,000 km is approximately 0.5 eV and the electron temperature is a few eV. *Tetrault* [1991] also bases his ion hole instability theory on the premise that $T_e/T_i \approx 1$ for auroral plasma. Investigating the response of our simulated plasma to the Alfvén wave for the case when $T_e \approx T_i$ required no modification of the model – it was simply a matter of changing the input parameters. As expected, the po-

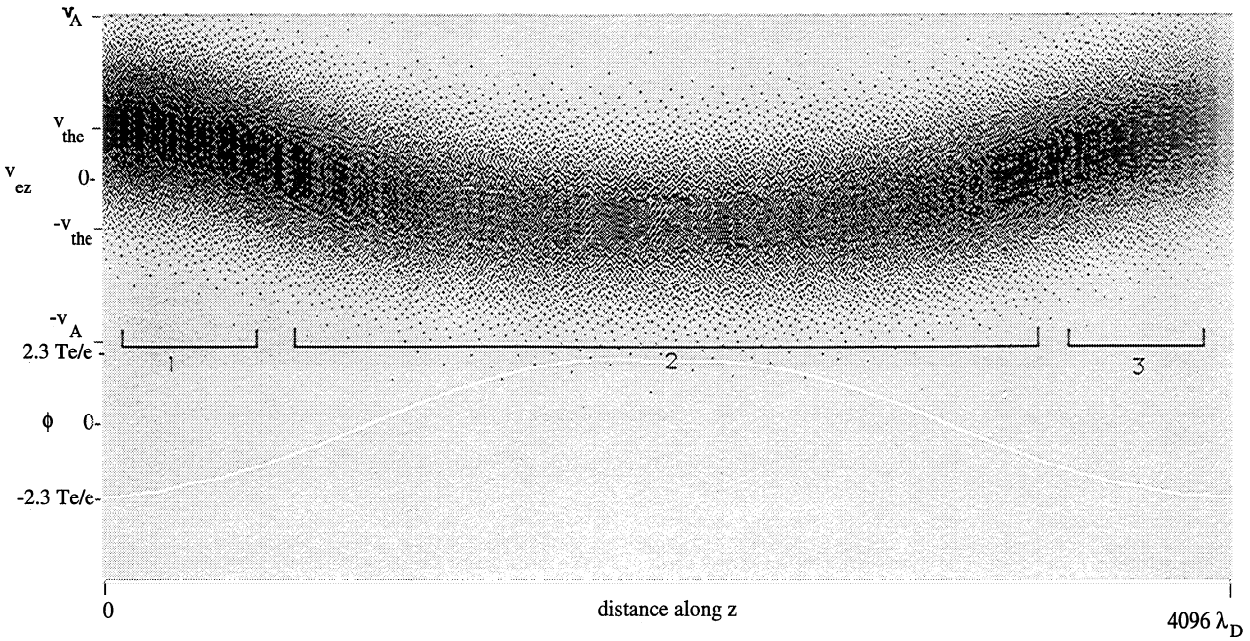

Figure 14. Initial electron phase-space configuration. The group of particles labeled 1 are initialized with the highest velocities; group 2 have velocities close to zero or negative; group 3 again have high velocities.

tential history, Figure 16 revealed the distinct absence of the ion-acoustic explosion and associated double layers, compared with the previous runs where T_e exceeded T_i. However, the macroscopic dynamics of the electron acceleration Figures 12 and 15 remained unchanged.

This is an especially important result. First of all, we can be fairly confident that the double layers in our simulation originate from the ion-acoustic instability and not from Tetrault's ion hole instability; when the ion-acoustic instability was removed, the double layers disappeared. More importantly, the inertial Alfvén wave, as an acceleration mechanism, acts separately from the double layers. Recall that the ion-acoustic instability required, in addition to $T_e \gg T_i$, a drift of electrons

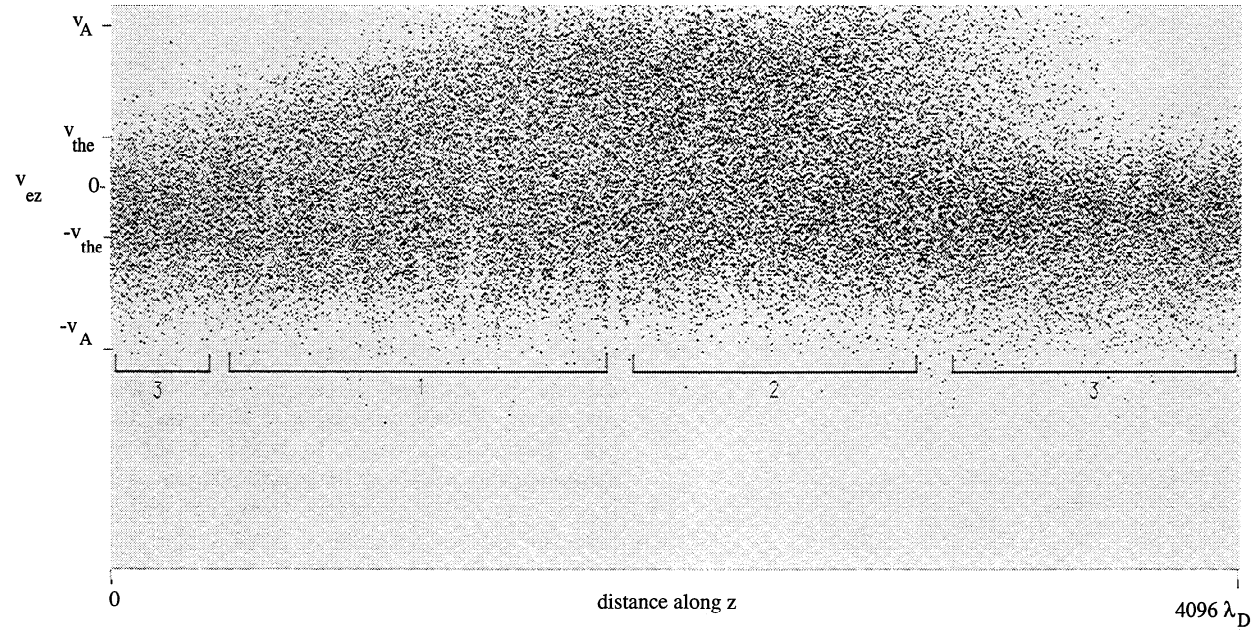

Figure 15. Acceleration of electrons as Alfvén wavefront passes through the distribution from left to right. The slowest electrons are accelerated, appearing in the wavefront, while the faster electrons are decelerated and then recycled. Electron heating is indicated by the widening velocity distribution.

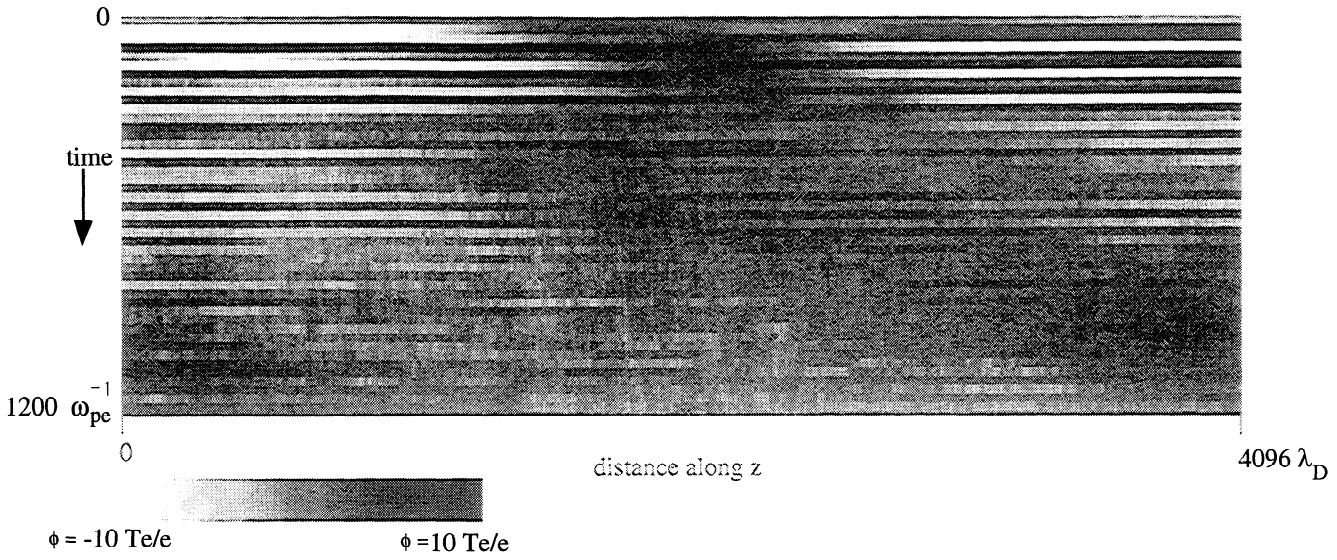

Figure 16. Potential history plot without ion-acoustic instability shows no double layers.

with respect to ions, produced partly by the inertial Alfvén wave and partly by an initial imposed drift. The contribution to the total drift motion is the only connection between the Alfvén wave and the double layers. Otherwise, the presence or absence of double layers is irrelevant with regard to electron acceleration. Moreover, if the ion-acoustic instability truly does not occur in this case, we cannot attribute the deceleration of electrons out of the beam to ion-acoustic turbulence. Plasma oscillations, an electron-electron two-stream instability, or the Buneman instability may account for this effect (C. Seyler, private communication [1992]).

Energy Transfer and Velocity Distribution

The exchange of energy between the wave and the particles was investigated numerically with a simple calculation. The field energy was calculated as $(B^2 + E^2)/8\pi$, averaged in Fourier space, and compared with the average kinetic energy of the particles. The energy transfer is illustrated in Figure 17. Here, we can clearly see the particles gaining energy at the expense of the wave. A plot of the distribution of particle velocities serves as a final diagnostic. The before and after plots in Figure 18 show the emergence of a distinct shoulder in the Maxwellian distribution, coinciding with the development of the steepening wave front we observed in the electron phase space plot. This shoulder is the beam we discussed earlier, together with a population of electrons generated by turbulence, filling in the gap between the beam and the main population. The distribution function appears almost immediately as a shoulder because there is constant recycling of particles between the beam and the main distribution. Later, the distribution thermalizes, as we would expect. Clearly, more electrons attain higher velocities as the Alfvén wave propagates through the system.

Conclusions

A simulation model has been developed to include, self-consistently, microscale processes together with their free energy source. Fully nonlinear kinetic parallel electron and ion dynamics are modeled together with an inertial Alfvén wave. Double layers form in the auroral current channel, owing to the evolution of an ion-acoustic instability energized by the wave. Tracking single-particle trajectories through and around double layers showed that double layers affect ion motion but have little bearing on large-scale electron dynamics. The ions performed the expected trapping motion and acceleration, and our observations of ion holes were consistent with those described in the literature. Large-scale electron motion was only slightly, if at all, affected

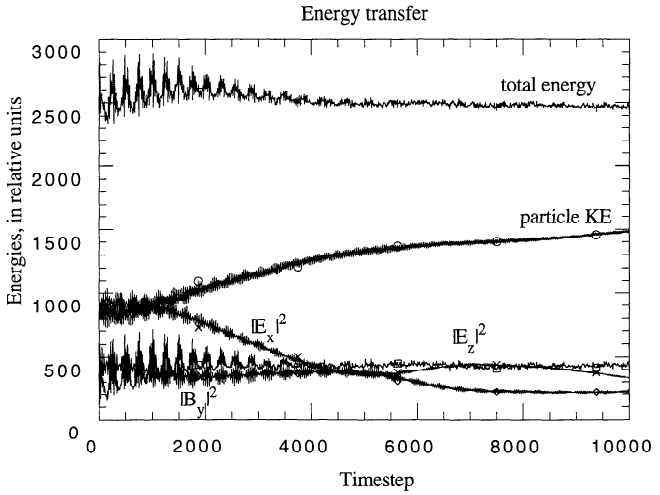

Figure 17. Energy exchange between the inertial Alfvén wave and the plasma particles. The field energies are averaged over the grid. The plot is consistent with total energy conservation.

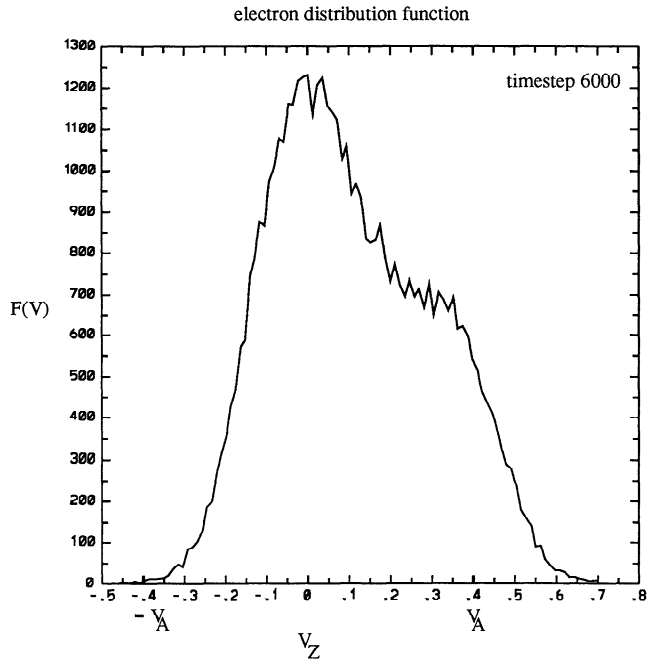

Figure 18. Electron velocity distribution function versus velocity, showing the distribution at time $720\,\omega_p e^{-1}$. Initial distribution at time 0 was a drifting Maxwellian with $v_d = v_{the} = 0.12$, and $v_A = 3.33 v_{the}$. The average electron velocity has decreased, while a portion of the electrons have been accelerated to the Alfvén speed.

by the double layers. Electrons first thought to exhibit trapping between double layers are more likely to be encountering resistance through an interaction with large amplitude plasma oscillations, turbulence brought about by an ion-hole instability or the electron-electron two-stream instability. The auroral electrons were otherwise oblivious to the presence of the double layers they encountered.

These observations imply that precipitating electrons are not energized primarily by double layers. Simulation movies clearly showed the inertial Alfvén wave accelerating the electrons into a beam. The beam particles are constantly interchanged with the main distribution as they are accelerated and then decelerated by small-scale, large-amplitude field fluctuations. The electrons do not free-stream across the length of the channel, thus suggesting that the electrons at the ionospheric boundary may not originate at high altitudes (i.e., at the plasma sheet) but are instead locally energized as the wave encounters them. When the electron and ion temperatures were comparable, the ion-acoustic explosion did not occur and double layers were conspicuously absent. Nevertheless, the wave still developed into a beam, while the electron motion remained unaffected by the temperature difference, demonstrating that with regard to electron acceleration, double layers are merely a passive consequence of the Alfvén-wave powered instability.

Acknowledgments. We are grateful to C. E. Seyler and C. H. Hui for insightful discussions and acknowledge the contributions of P. Gray to the design of the original model. We appreciate the comments of P. M. Kintner, A. Koskinen, T. Chang, A. Malkii, and M. K. Hudson. This work was made possible by NASA grant NAGW-2011 and was further supported under the NSF GEE Fellowship program and by the USAFA Physics Department in conjunction with AFIT/CI.

The Editor thanks M. A. Temerin and J. E. Borovsky for their assistance in evaluating this paper.

References

Barnes, C., M. K. Hudson, and W. Lotko, Weak double layers in ion acoustic turbulence, *Phys. Fluids*, *28*, 1055, 1985.

Birdsall, C. K., and A. B. Langdon, *Plasma Physics via Computer Simulation*, McGraw-Hill, New York, 1985.

Borovsky, J. E., 1991. Strong double layers and auroral arcs: An overview and assessment. Paper presented at Chapman Conference on Auroral Plasma Dynamics, AGU, Minneapolis, Minn., Oct. 21-25, 1991.

Bostrom, R., G. Gustafsson, B. Holback, G. Holmgren, H. Koskinen, and P. Kintner, Characteristics of solitary waves and weak double layers in the magnetospheric plasma, *Phys. Rev. Lett.*, *61*, 82, 1988.

Chan, C., N. Hershkowitz, A. Ferreira, T. Intrator, B. Nelson, and K. Lunngren, Experimental observations of self-similar plasma expansion, *Phys. Fluids*, *27*, 266, 1984.

Goertz, C. K., and R. W. Boswell, Magnetosphere-ionosphere coupling, *J. Geophys. Res.*, *84*, 7239, 1979.

Goertz, C. K., T. Whelan, and K. I. Nishikawa, A new numerical code for simulating current-driven instabilities on auroral field lines, *J. Geophys. Res.*, *96*, 9579, 1991.

Hasegawa, A., Particle acceleration and mhd surface wave and formation of aurora, *J. Geophys. Res.*, *81*, 5083, 1976.

Hasegawa, A., and L. Chen, Kinetic process of plasma heating due to alfven wave excitation, *Phys. Rev. Lett.*, *35*, 370, 1975.

Hasegawa, A., and T. Sato, Existence of a negative potential solitary wave structure and the formation of a double layer, *Phys. Fluids*, *25*, 632, 1982.

Hudson, M. K., T. L. Crystal, W. Lotko, and C. Barnes, Weak double layers in the auroral ionosphere, *Lasers and Particle Beams*, *5*, 295, 1987.

Hudson, M. K., W. Lotko, I. Roth, and E. Witt, Solitary waves and double layers on auroral field lines, *J. Geophys. Res.*, *88*, 916, 1983.

Koskinen, H., R. Lundin, and B. Holback, On the plasma environment of solitary waves and weak double layers, *J. Geophys. Res.*, *95*, 5921, 1990.

Lysak, R. L., and C. T. Dum, Dynamics of magnetosphere-ionosphere coupling including turbulent transport, *J. Geophys. Res.*, *88*, 365, 1983.

Mälkii, A., R. Boström, P. O. Dovner, A. I. Eriksson, and G. Holmgren, Viking observations of weak double layers and solitary structures in the auroral acceleration region: Latest results, *EOS Trans., AGU*, *73*, 43, 1992.

Mozer, F. S., C. A. Cattell, M. K. Hudson, R. C. Lysak, M. Temerin, and R. B. Torbert, Satellite measurements and theories of low altitude auroral particle acceleration, *Space Sci. Rev.*, *27*, 155, 1980.

Otani, N. F., 1991. Particle simulation of the interaction between kinetic Alfvén waves and double layers. In *Modeling of Magnetospheric Plasma Processes, Geophys. Monogr. Ser.*, volume 62, edited by G. R. Wilson, p. 95, AGU, Washington, D. C., 1991.

Sato, T., and H. Okuda, Numerical simulations on ion acoustic double layers, *J. Geophys. Res.*, *86*, 3357, 1981.

Seyler, C. E., Nonlinear 3-d evolution of bounded kinetic alfvén waves due to shear flow and collisionless tearing instability, *Geophys. Res. Lett.*, *15*, 756, 1988.

Stefant, R. J., Alfvén wave damping from finite gyroradius coupling to the ion acoustic mode, *Phys. Fluids*, *13*, 440, 1969.

Swift, D. W., On the formation of auroral arcs and acceleration of auroral electrons, *J. Geophys. Res.*, *80*, 2096, 1975.

Temerin, M., K. Cerny, W. Lotko, and F. S. Mozer, Observation of double layers and solitary waves in auroral plasma, *Phys. Rev. Lett.*, *48*, 1175, 1982.

Tetrault, D. J., Growing ion holes as the cause of auroral double layers, *Geophys. Res. Lett.*, *15*, 164, 1988.

Tetrault, D. J., Theory of electric fields in the auroral acceleration region, *J. Geophys. Res.*, *96*, 3549, 1991.

N. F. Otani and M. Silberstein, School of Electrical Engineering, Cornell University, Ithaca, New York 14853

(Received December 3, 1992; revised October 15, 1993; accepted October 19, 1993.)